ANU-P/1095
June 1991

# DYNAMICS OF FISSION AND QUASI-FISSION REVEALED BY PRE-SCISSION NEUTRON EVAPORATION

D.J. Hinde

Department of Nuclear Physics, Research School of Physical Sciences,
Australian National University, GPO Box 4, Canberra ACT 2601, Australia

D. Hilscher and H. Rossner

Hahn-Meitner-Institut Berlin, D-1000 Berlin 39, Germany

Accepted for Publication in
Nucl Phys A, June 1991

ANU P1095
4 June 1991

# DYNAMICS OF FISSION AND QUASI-FISSION REVEALED BY PRE-SCISSION NEUTRON EVAPORATION

D. J. Hinde

Department of Nuclear Physics, Australian National University,
GPO Box 4, Canberra, ACT 2601, Australia

D. Hilscher and H. Rossner

Hahn-Meitner-Institut Berlin, D-1000 Berlin 39, Germany

The dependence of pre-scission neutron multiplicities ( $\nu_{pre}$ ) on the mass-split and total kinetic energy in fusion-fission and quasi-fission has been measured for a wide range of projectile-target combinations. The data indicate that the fusion-fission time scale is shorter for asymmetric splits than for symmetric splits, whilst there is no dependence on TKE. For quasi-fission reactions induced using $^{64}$Ni projectiles, $\nu_{pre}$ falls rapidly with increasing TKE, indicating that these neutrons are emitted near to or after scission. A new interpretation of both neutron multiplicities and mean energies ( the *neutron clock- thermometer* ) allo vs the extraction of time scales with much less uncertainty than previously, and also gives information about the deformation from which the neutrons are emitted.

## 1. INTRODUCTION

Detailed experimental investigations of the characteristic time scales associated with non-grazing nucleus-nucleus collisions have historically proceeded from the most rapid and peripheral ( deep inelastic collisions, $\sim 10^{-21}$ s ), through reactions generally intermediate in time and impact parameter ( quasi-fission, $\sim$ several $10^{-21}$ s), to the most central and slowest process, fusion-fission ($> 10^{-20}$ s). This reflects the experimental problems in determining the long reaction times for the latter process, where the identities of the projectile and target nuclei are completely

lost, and no information can be obtained from the angle of observation of the fragments, unlike in the more rapid reactions. Their time scales are determined by the dynamics of the energy loss process and the mass-equilibration process, competing with the Coulomb repulsion forcing the nascent fragments apart.

It used to be considered that fusion-fission was ruled by phase space, by extension from the approach used in fission at low excitation energies. However at high thermal excitation energies ( $E_x$ ), and/or for fissile systems, this would imply lifetimes of less than $10^{-21}$ s. Through various theoretical approaches, it has been shown that the typical minimum time for the nucleus to proceed from the equilibrium deformation to scission is several $10^{-21}$ s, this time increasing for both higher and lower nuclear viscosity.

Experimental evidence for the slow fission time scale has come from measurements of the numbers of evaporated neutrons[1], charged particles[2] and giant dipole $\gamma$-rays[3] emitted before scission, which are generally in excess of those predicted using static phase space arguments alone ( the statistical model ). It may be argued that the dominance of the neutron channel in most systems studied in this context, and the absence of a Coulomb barrier, leads to fewer uncertainties in determining time information from pre-scission neutron multiplicities ( $\nu_{pre}$ ). Of course very valuable complementary evidence has been obtained from studies of other evaporation channels, particularly in conjunction with neutron data, and in the future it may be that charged particle emission will be able to give more detailed information on fission dynamics through the greater sensitivity to nuclear shape.

The total dynamical fission time scale, from thermal equilibration to scission ( $\tau_f$ ) is in principle obtained using the relation

$$\tau_f = \sum_{i=1}^{\nu_{pre}} \frac{\hbar}{\Gamma_i},$$

and with neutrons dominant,

$$\Gamma_i \approx \Gamma_n(E_x, I) = \frac{(2s_n+1)}{2\pi\rho(E_x, I)} \sum_{l=0}^{\infty} \sum_{J=I-l}^{J=I+l} \int_0^{E_x - B_n} \rho(E_x - B_n - \epsilon_n, J) T_l(\epsilon_n) d\epsilon_n.$$

This has been called[1] the *neutron clock*, but the clock rate depends strongly on the level density $\rho$, normally taken for a nucleus with angular

momentum $J\hbar$ to have the form

$$\rho(E_x, J) \propto \frac{(2J+1)}{(E_x)^2} exp(2\sqrt{a_n E_x}).$$

Thus the clock rate depends sensitively on the level density parameter for neutron emission $a_n$ and the thermal excitation energy $E_x$ ( the energy above the ground-state minus rotational and deformation energy ). Nevertheless, using reasonable assumptions, values of $\tau_f$ of several $10^{-20}$ s have been deduced from measured $\nu_{pre}$ data[4].

In an attempt to gain a better understanding of both fusion-fission and quasi-fission, a series of measurements were carried out at the Hahn-Meitner-Institut, Berlin, where pre- and post-scission neutron multiplicities were measured for 27 reactions using beams of 158.8 MeV $^{18}$O, 288.0 MeV $^{16}$O, 249.0 MeV $^{40}$Ar and 417.7 MeV $^{64}$Ni, incident on a range of targets, as a function of the fission mass-split, total kinetic energy (TKE), and in one case, as a function of fragment angle. This program has resulted in a total of 248 new data points. Statistical model analyses and interpretation of these results have been carried out at the Australian National University, Canberra.

Due to the extensive data, only certain of the most interesting results can be shown here. Those for fusion-fission reactions will be presented first, followed by those for quasi-fission. An interpretation of these measurements will then be made, using an extension of the neutron clock, which it may be appropriate to call the *neutron clock-thermometer.*

## 2. FUSION-FISSION

### 2.1 TKE Dependence of $\nu_{pre}$

Neutron multiplicities are determined from a measured neutron angular correlation using a multiple moving source fitting procedure. In this work, the most critical input parameters, namely the fission fragment velocity vectors, were determined experimentally. However, it has been shown[5] that in fitting angular correlations obtained by applying cuts to the measured TKE ( but *not* cuts in mass ), neglect of neutron recoil effects causes an apparent strong dependence of $\nu_{pre}$ on TKE. This is best illustrated in Fig.1. Here, computer-generated neutron angular correlations, calculated for $\nu_{pre}$ =0.8, independent of TKE as shown by the small

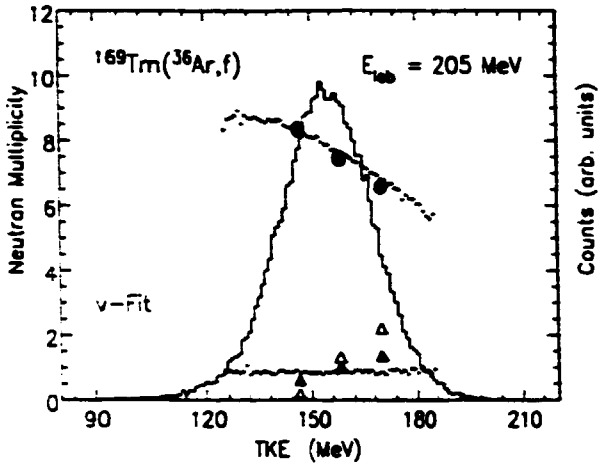


Figure 1: Fitted neutron multiplicities from computer-generated data for the reaction indicated. Hollow ( solid ) triangles and circles show values of $\nu_{pre}$ and $\nu_{tot}$ respectively determined without (with ) application of the main neutron recoil correction. The small diamonds show the corresponding values used as input.

points, have been fitted with a multiple-source fit ignoring any neutron recoil effects. A strong dependence of $\nu_{pre}$ on TKE is seen ( hollow triangles ). By exactly correcting for the principal recoil effect in the fitting program, the solid points were obtained, which show that 0.7 of the total neutron recoil effect is accounted for. Then by applying the correction increased by a factor 1.4, the input $\nu_{pre}$ value can be reproduced.

Turning now to the experimental data, the dependence of $\nu_{pre}$ and $\nu_{tot}$ for the reactions of 158.8 MeV $^{18}$O + $^{154}$Sm, $^{197}$Au are shown in Fig.2. The lower panels of the figure show the cuts applied in the mass-TKE matrix to obtain the results in the upper panels. In order to maintain a similar distribution of fragment masses in each gate, a *relative TKE* ( RTKE ) was generated, using the Viola systematics[6] modified to give the TKE for different mass-splits.

$$RTKE = \frac{TKE}{\left(\frac{0.755 Z_1 Z_2}{(A_1^{1/3}+A_2^{1/3})} + 7.3\right)}.$$

Linear cuts in RTKE gave the curved gates in TKE shown in the figure. The values of $\nu_{pre}$ shown by hollow circles were obtained by fitting the data neglecting neutron recoil effects, the solid circles by including the main recoil effect, and the stars by increasing the correction by the factor 1.4, determined from fitting the computer-generated results discussed above. These last points show no dependence on TKE within experimen-

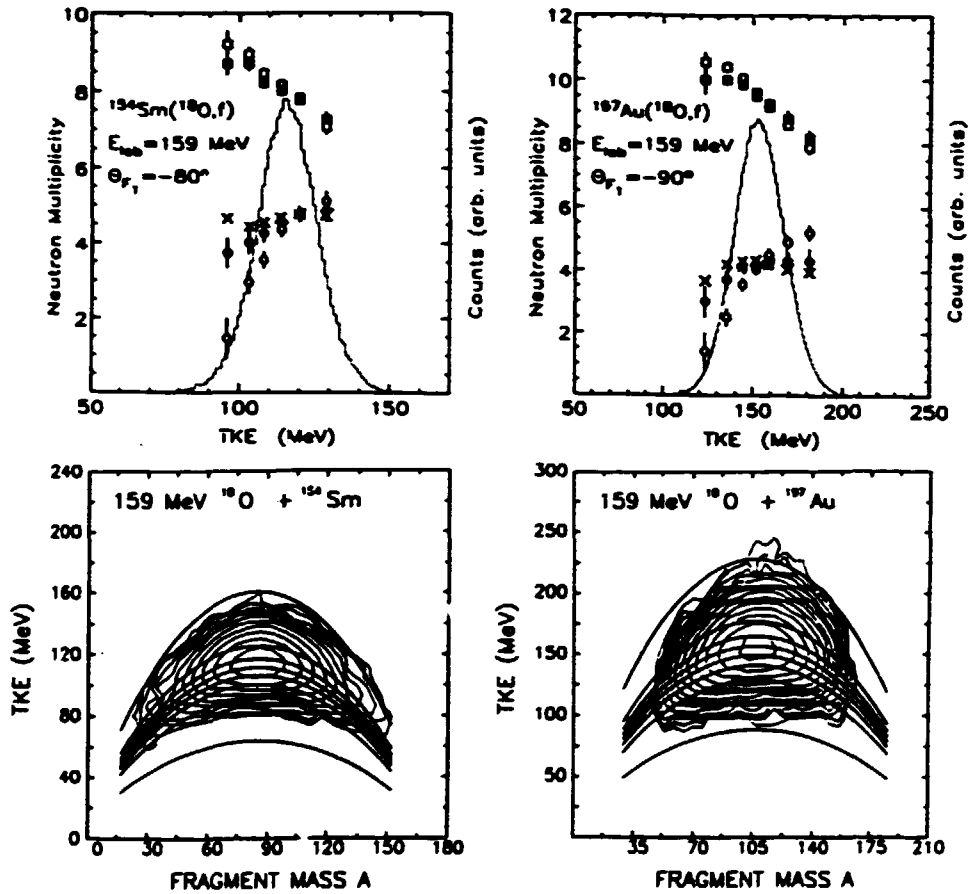


Figure 2: The lower panels show the singles fission yield in fragment mass and TKE, contour lines represent a factor of 1.414 change in yield. The mass and TKE are determined from the measured mass-split and fragment velocities assuming no evaporated particles, thus symmetric fission corresponds to half the compound nucleus mass. Cuts in RTKE result in the curved gates corresponding to the data points in the upper panels. Deduced values of $\nu_{pre}$ and $\nu_{tot}$ ( squares ) are shown for different fitting conditions ( see text ).

tal error, which is consistent with expectations for fusion-fission.

## 2.2 Mass-Asymmetry Dependence of $\nu_{pre}$

The dependence of $\nu_{pre}$ and $\nu_{tot}$ on the fission mass-split is shown in Fig.3, for the same reactions as in Fig.2. The mass cuts applied are shown in the lower panels. Somewhat surprisingly, $\nu_{pre}$ shows a very strong dependence on mass-split, at least as large as the variation of $\nu_{tot}$ . The latter is caused by energy balance, due to the variation with mass-asymmetry of the effective fission Q-value ( $Q_f$ ), which is defined in terms of the masses of the compound nucleus and the fission fragments

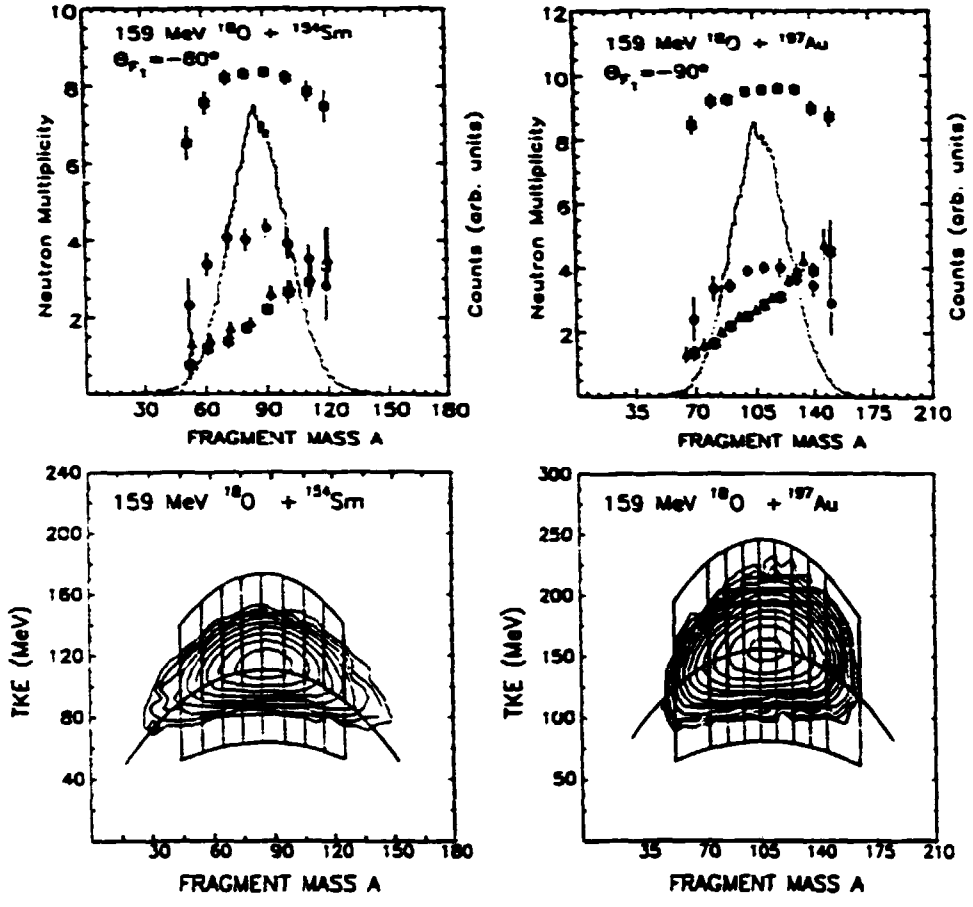


Figure 3: The lower panels show the calculated TKE according to the Viola systematics, and the gates corresponding to the multiplicities in the upper panels, where the projected mass-distribution is shown, together with the fitted values of $\nu_{pre}$ and $\nu_{tot}$ as a function of fragment mass, shown by the filled circles and squares respectively, and $\nu_{post}$ for the two fragments, shown by hollow triangles and squares.

( $M_{CN}$, $M_{f_1}$ and $M_{f_2}$ ) and the mass-asymmetry dependent TKE:

$$Q_f = M_{CN} - (M_{f_1} + M_{f_2} + TKE).$$

The effect of $Q_f$ itself is only felt strongly by the system near and after scission, so it should not have a significant influence on $\nu_{pre}$ in fusion-fission, although the potential energy surface ( PES ) will be correlated with $Q_f$ to some extent. The variation of $\nu_{pre}$ with mass-asymmetry can be explained qualitatively as a combination of three effects.

Due to fluctuations in the dynamical pre-saddle delay time and the random nature of the decay process, there will be variations from nucleus to nucleus in the number of neutrons emitted before the fission barrier is being surmounted. Those nuclei with the highest excitation energy

are more likely to pass over the higher mass-asymmetric barriers. Once the mass-asymmetry is defined, and assuming that it does not change appreciably, asymmetric systems will have a lower $E_x$ , longer neutron lifetimes and thus will emit fewer neutrons on the path from saddle to scission. Thus higher barriers ( lower fission yields ) should be correlated with lower values of $\nu_{pre}$ .

The third, and most interesting cause, is that the dynamical fission time scale $\tau_f$ may reasonably be expected to be shorter for asymmetric fission. This can be disentangled from the former phase space arguments by choosing a light compound nucleus near the Businaro-Gallone point, where there is no dependence of fission barrier height on mass-asymmetry, so variation of $\nu_{pre}$ should be solely due to variation of $\tau_f$ .

The reaction of 288 MeV $^{16}$O with $^{109}$Ag was expected from systematics[7] to show a rather flat fission mass-distribution. The measured mass-yield, given in Figs. 4a,4b, shows that this was the case. A narrow cut in RTKE was made as shown to select fusion-fission events, and to minimise the possibility of complementary fragments being deflected out of the angular range of that fission detector. The mass-distribution for this cut is shown by the histogram, together with the deduced neutron multiplicities. The $\nu_{tot}$ values do show a reduction for asymmetric mass-splits; this is emphasised in Fig.4c, where $\nu_{pre}$ only is shown as a function of the mass of the light fragment. Applying the *neutron clock* principle, including emission of charged particles, ( implemented in a heavily modified version of the Monte-Carlo code JULIAN[5] in the form of a period of time during which fission is totally suppressed but evaporation proceeds normally ) allows $\tau_f$ to be determined for each mass bin, as shown in Fig.4d. The values extracted for symmetric fission are within experimental error in agreement with those deduced for heavier nuclei ( see Section 4 ), whilst there is a marked decrease in $\tau_f$ for asymmetric fission. This evidence is supported by the results[8,9] from a similar reaction at higher energy, where for intermediate mass fragments ( IMF ) of mass $\sim$ 20, the delay time between the emission of two IMFs, and the delay before IMF emission, were determined by the Coulomb correction method and from multiplicity distributions respectively. These gave times $\tau_f$ of 0.8 and $1.7 \times 10^{-21}$ s respectively, the average being shown by the star in the figure. Considering the uncertainties in each method, the agreement is

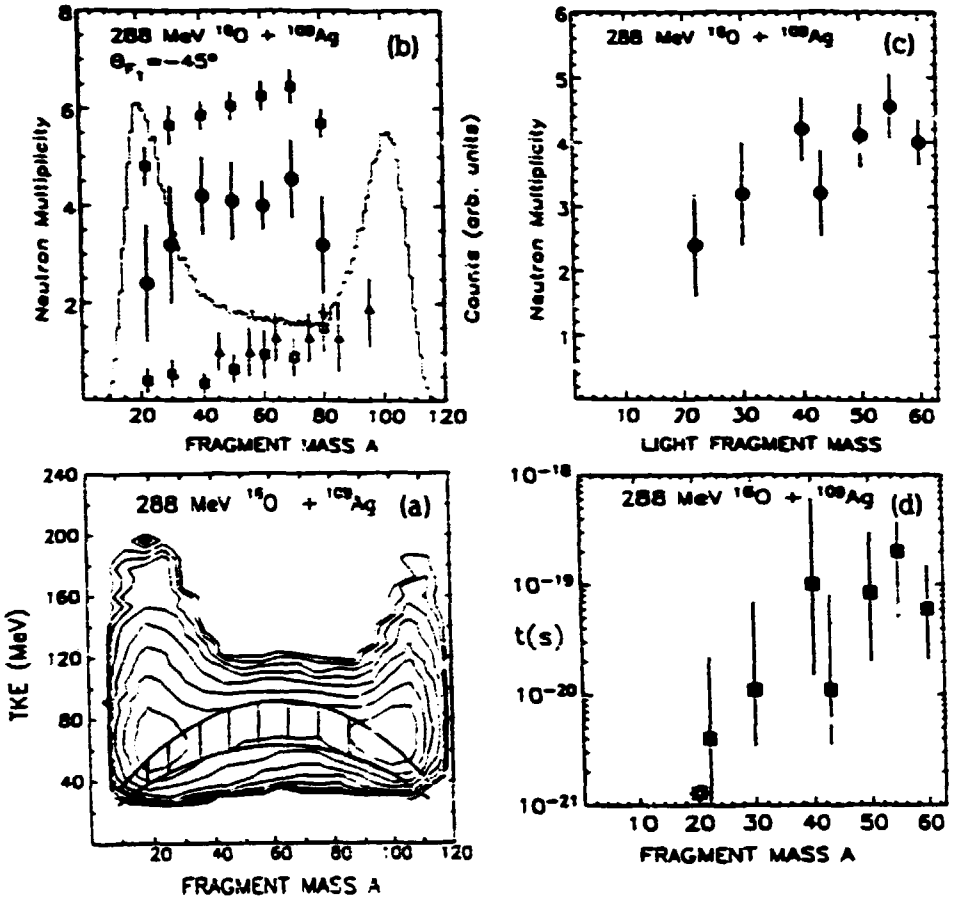


Figure 4: Panel (a) shows the gates applied to the mass-TKE matrix corresponding to the fitted points in panel (b), where the projected mass-distribution is shown, together with the fitted values of $\nu_{pre}$ , $\nu_{post}$ and $\nu_{tot}$ , shown by the filled circles, hollow squares and triangles, and filled squares respectively. Panel (c) shows $\nu_{pre}$ only, whilst panel (d) shows the deduced $\tau_f$ values ( see text ).

gratifying.

Such a variation of $\tau_f$ with mass-asymmetry makes more reasonable the hypothesis[10] that fission and evaporation are the extremes of a unified binary decay mechanism, since their different characteristics can be associated with the change in characteristic time scale with asymmetry.

## 3. QUASI-FISSION

The reaction of $^{40}$Ar with $^{238}$U and $^{208}$Pb have been placed in the quasi-fission category, since an asymmetry in the fragment mass-yield at forward angles was observed, characteristic of quasi-fission.

The very wide mass-yields for the $^{64}$Ni-induced reactions shown later

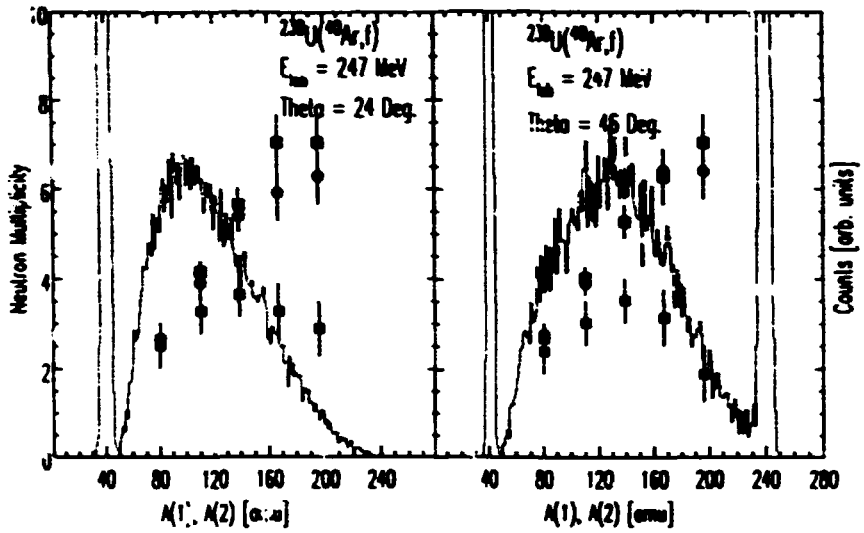


Figure 5: Observed mass yields for reaction and angles as indicated, together with the fitted values of $\nu_{pre}$ , shown by the filled squares. $\nu_{post}$ for both fragments are shown as a function of the mass ( A(1) ) of the fragment seen at the indicated angle and of the mass of the complementary fragment ( A(2) ), by hollow circles and squares respectively.

make it clear that quasi-fission is the dominant process.

### 3.1 Mass-Asymmetry Dependence of $\nu_{pre}$

The variations of $\nu_{pre}$ with mass-split for the $^{40}$Ar + $^{238}$U reaction at two fragment detection angles ( 24 and 46 degrees ) are shown in Fig.5, together with the observed mass-yields. The same parabolic dependence on asymmetry is seen here as in fusion-fission reactions, but in quasi-fission, the fission barrier does not play a rôle, so the multiplicities should be determined by the PES and the reaction time scale alone. Within experimental error, the value of $\nu_{pre}$ for a given asymmetry is independent of the observed mass, as in fusion-fission, suggesting that at angles close to the beam direction, the lighter fragment does not originate from faster reactions. This question will be further discussed in Section 4.

For the reactions of 417.7 MeV $^{64}$Ni with $^{154}$Sm, $^{175}$Lu, $^{197}$Au, $^{208}$Pb and $^{238}$U, broad mass-distributions extending from projectile to target mass were observed. The measurements were made at angles close to 90 degrees in the centre-of-mass frame, examples of the experimental mass-TKE data being shown in Fig.6. The fitted values of $\nu_{pre}$ again show a parabolic dependence on mass, whose explanation must be the same as for the $^{40}$Ar data. The post-scission multiplicities from both fragments are consistent with a sharing of energy at scission proportional to mass,

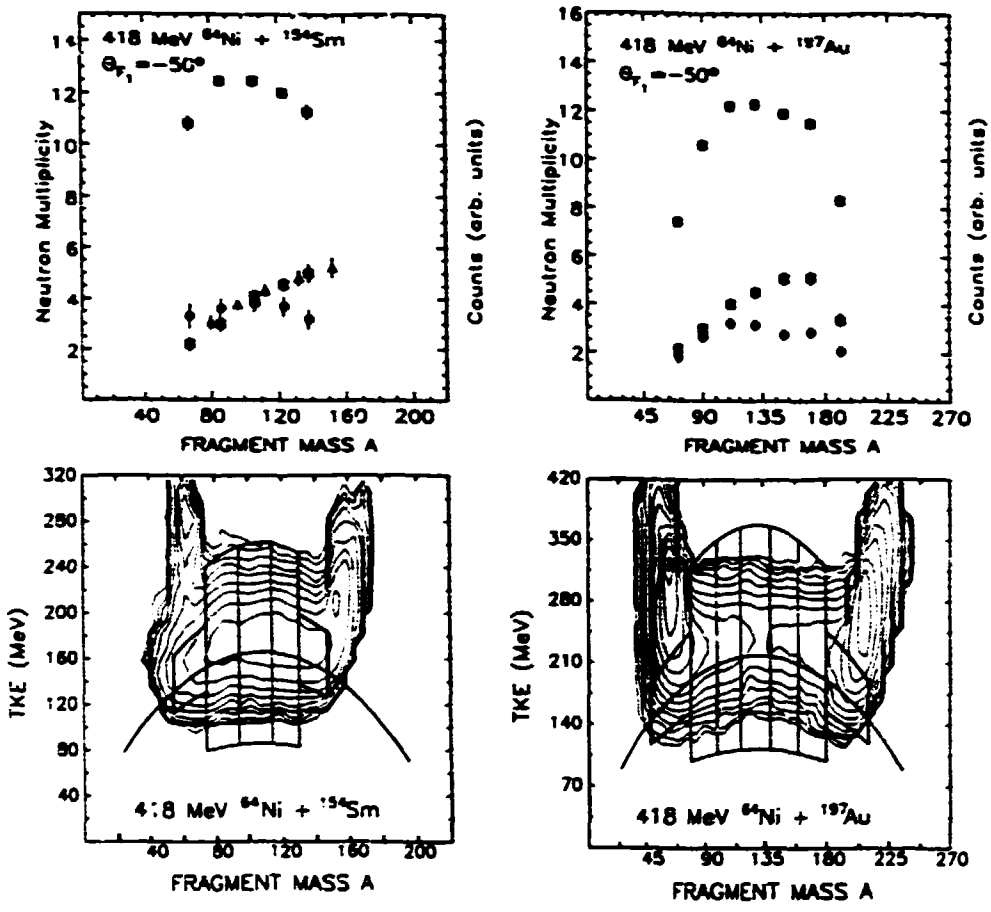


Figure 6: The lower panels show the measured mass-TKE matrix for the reactions indicated. Contour lines correspond to a factor of 2 change in yield. Also shown are the cuts in mass and RTKE applied to obtain the neutron angular correlations as a function of mass-split. The multiplicities obtained from fitting the latter are shown above, filled circles corresponding to $\nu_{pre}$ , hollow points to $\nu_{post}$ and filled squares to $\nu_{tot}$ .

as was the case in the fusion-fission reactions. This must reflect the fact that the reaction is sufficiently slow to allow thermal equilibration to take place. For the reaction of $^{64}$Ni with $^{238}$U at similar energies, measurement of the fission angular distribution allowed[11] the sticking time, which we can identify with $\tau_f$ , to be estimated at $\sim 6\times 10^{-21}$ s. For reaction times of this order, it may seem that the measured values of $\nu_{pre}$ are rather large. This point will be addressed in the next section.

### 3.2 TKE Dependence of $\nu_{pre}$

For all the reactions with $^{64}$Ni projectiles, it was found that there was a very strong dependence of $\nu_{pre}$ on TKE, as is illustrated in Fig.7. Even without the neutron recoil correction, $\nu_{pre}$ decreases rapidly with TKE,

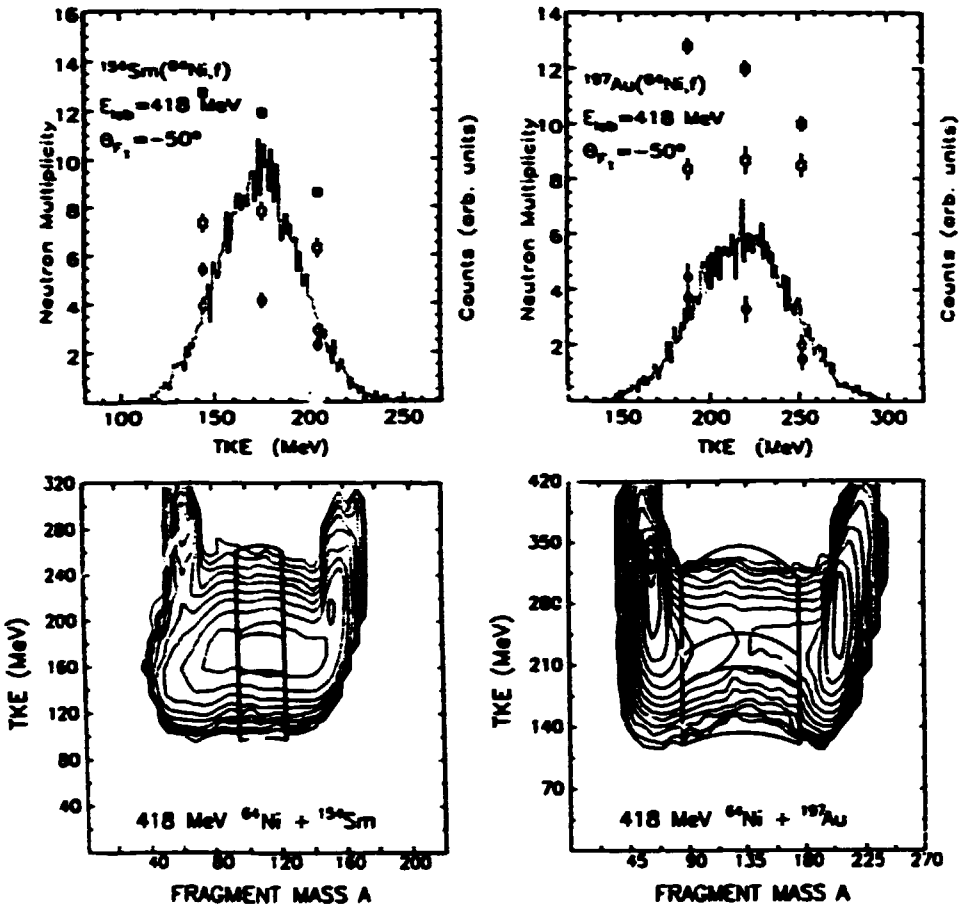


Figure 7: The lower panels show the cuts in mass and RTKE applied to obtain the neutron angular correlations as a function of TKE. The multiplicities obtained from fitting the latter are shown above, filled circles corresponding to $\nu_{pre}$ , hollow squares to $\nu_{post}$ and filled squares to $\nu_{tot}$ .

in contrast with the fusion-fission data. Including the correction gives an even stronger effect. Conversely, for the $^{40}$Ar + $^{238}$U reaction, the results are more like fusion-fission, with an increase of $\nu_{pre}$ with TKE before neutron recoil corrections are applied; preliminary results taking into account the recoil effect indicate a very slight reduction of $\nu_{pre}$ with increasing TKE. Deduced values of $\tau_f$ for similar reactions[11] with Uranium are about twice those for the $^{64}$Ni-induced reaction; this evidence, together with the more asymmetric mass-distributions suggests that the composite nucleus ( mononucleus ) formed in the $^{64}$Ni reactions does not reach the same degree of compactness as in the $^{40}$Ar + $^{238}$U reaction.

The observed strong dependence of $\nu_{pre}$ on TKE is probably caused by two effects. Assuming that a mononucleus is formed with a given elongation, the Coulomb repulsion of the two halves will tend to increase the

elongation. Random shape fluctuations may lead to snapping of the neck early or late in the time evolution: early should be correlated with high TKE, and the short time and low $E_x$ will lead to low multiplicity, whilst late will be correlated with low TKE, and the longer time and higher $E_x$ will result in a high multiplicity. The second effect is that of emission during acceleration of the fragments. It has been shown[12] that for short lifetimes and large positive values of $Q_f$ , this is an important effect which is not taken into account in the multiple source fitting procedure. It was shown that the neutron multiplicity emitted from the fragments in the first $\sim 2.5\times 10^{-21}$ s, during which they reach $\sim$ 0.8 of their asymptotic velocity, appears in the fit as part of the pre-scission component, due to the incomplete focussing of neutrons emitted before the fragments approach their final velocity. Again, due to energy balance, low TKE will be correlated with high $E_x$ , short neutron emission lifetimes and a larger multiplicity, whilst high TKE will result in a low multiplicity. Thus *acceleration neutrons* will also contribute to the observed gradient.

Quantitative calculations will be made in the next Section.

## 4. THE NEUTRON CLOCK-THERMOMETER

It has been shown in the introduction that the *neutron clock* is sensitive to $a_n$ and $E_x$ . During the fission process, the nucleus passes over the PES, which varies substantially in height between the equilibrium deformation and scission, thus $E_x$ will vary from that at the equilibrium deformation ( $E_x^0$ ). This is shown schematically in Fig.8 for both light and heavy nuclei. Particularly for the latter, $E_x$ may be very different from $E_x^0$ ; for the $^{40}Ar + ^{238}U$ reaction, neutron lifetimes are calculated to be $\sim$ 10 times shorter at the scission configuration, only considering the difference in excitation energy. The question is, what values of $E_x$ are appropriate, and without *a priori* knowledge of the trajectory over the PES, the uncertainty in $E_x$ for heavy systems would give little chance of reliably using the neutron clock.

Information on the nuclear temperature ( $T = \sqrt{E_x / a_n}$ ) is however carried by the neutron energy spectrum; it is well-known that the high-energy slope of an evaporation spectrum can be used to determine the T of the source. In these experiments, due to the presence of multiple

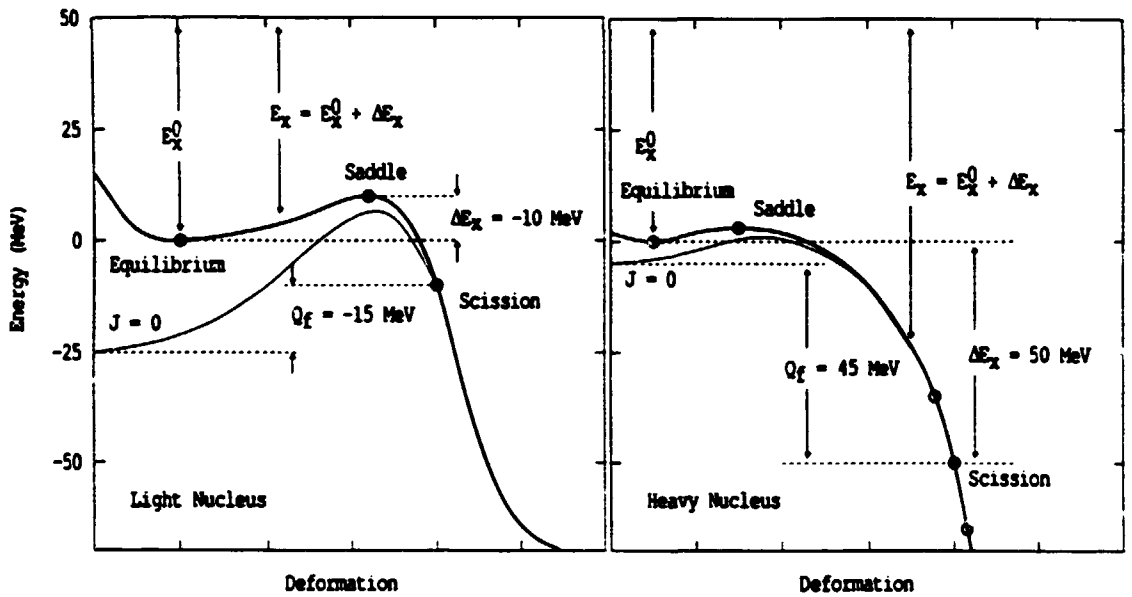


Figure 8: The potential energy surfaces ( PES ) of a light and a heavy nucleus shown schematically as a function of an arbitrary deformation parameter which corresponds to the lowest path between equilibrium and scission. The PES for zero angular momentum ( J = 0 ) and for a typical fissioning angular momentum ( heavy line ) are shown. The definition of $\Delta E_x$ and $Q_f$ are shown. They illustrate that for a light ( heavy ) nucleus, $\Delta E_x$ may be expected to be negative ( positive ), and that variations of the scission radius ( and thus TKE ) correspond to different $\Delta E_x$ .

neutron sources, the mean pre-scission neutron energy $\varepsilon_{pre}$ was a better defined quantity, given in principle by

$$\varepsilon_{pre} = \sum_{i=0}^{\nu_{pre}} \frac{\int_0^{E_x - B_n} \epsilon_n \Gamma_n(E_x, I, \epsilon_n) d\epsilon_n}{\Gamma_n(E_x, I)}.$$

Within the code JULIAN, where it is assumed that a cascade of neutrons originates from a given initial $E_x$ , that value was adjusted from the calculated $E_x^0$ ( determined by the fusion Q-value ) by an energy shift $\Delta E_x$ , such that $E_x = E_x^0 + \Delta E_x$ . Alternatively, variation of $a_n$ would have the same effect on T, and thus on $\varepsilon_{pre}$ , however because of the uncertainty in $E_x$ due to the PES, $a_n$ was fixed, the equation of ref.13 being used to define it for each compound nucleus ( thus it varied over the range $a_n = A/8.12$ to $a_n = A/9.15$ ). The parameters $\Delta E_x$ and $\tau_f$ were then treated as free parameters, and a lattice of calculated $\varepsilon_{pre}$ and $\nu_{pre}$ values was determined as a function of $\Delta E_x$ and $\tau_f$ for each reaction studied. An example is shown in Fig.9 for a fusion-fission reaction. Making use of the measured values of $\nu_{pre}$ and $\varepsilon_{pre}$ defines a narrow ac-

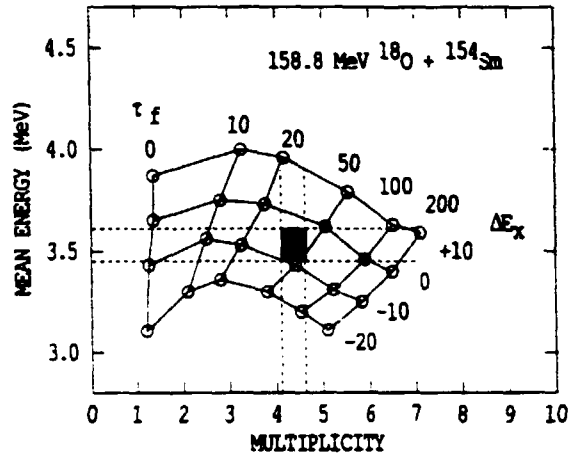


Figure 9: Calculated correlated values of $\nu_{pre}$ and $\varepsilon_{pre}$ for the reaction indicated, resulting from variation of $\tau_f$ between 0 and 200 $\times$ $10^{-21}$ s, and for $\Delta E_x$ between -20 and +10 MeV. The experimental datum is indicated by the black rectangle.

ceptable range of $\Delta E_x$ and $\tau_f$ values, whereas use of one experimental value only in principle defines neither. It is important to re-emphasise that variation of $a_n$ would change the deduced value of $\Delta E_x$ , *but not of* $\tau_f$ , as explained above.

In reality, each neutron will be emitted from a different point in deformation space, with a different $\Delta E_x$ ( see Fig.8 ), so the deduced $\Delta E_x$ in this analysis represents a complex average over the whole fission trajectory, which may result in some uncertainty in $\tau_f$ , nevertheless, this method represents a great improvement over previous analyses of $\nu_{pre}$ data, and the validity of requiring that *both* $\nu_{pre}$ and $\varepsilon_{pre}$ should be fitted is undeniable. This should be done in future analyses carried out with more sophisticated dynamical/evaporation computer codes.

### 4.1 Application to Fusion-Fission

Applying this approach to experimental data requires a reasonable initial choice of $E_x^0$ , if $\Delta E_x$ is to have any meaning beyond being a fitting parameter. For the 158.8 MeV $^{18}O$ reactions, the correctness of the value of $E_x^0$ was tested by calculating $\nu_{tot}$ for each reaction using JULIAN. The comparison of these values with measured results is shown in Fig.10. It is clear that $E_x^0$ was overestimated for the most fissile nuclei, probably due to fission following incomplete fusion. Nevertheless, the deduced $\Delta E_x$ and $\tau_f$ are shown for this initial condition by full circles in the right panels. Reducing $E_x^0$ to obtain agreement of $\nu_{tot}$ results in a

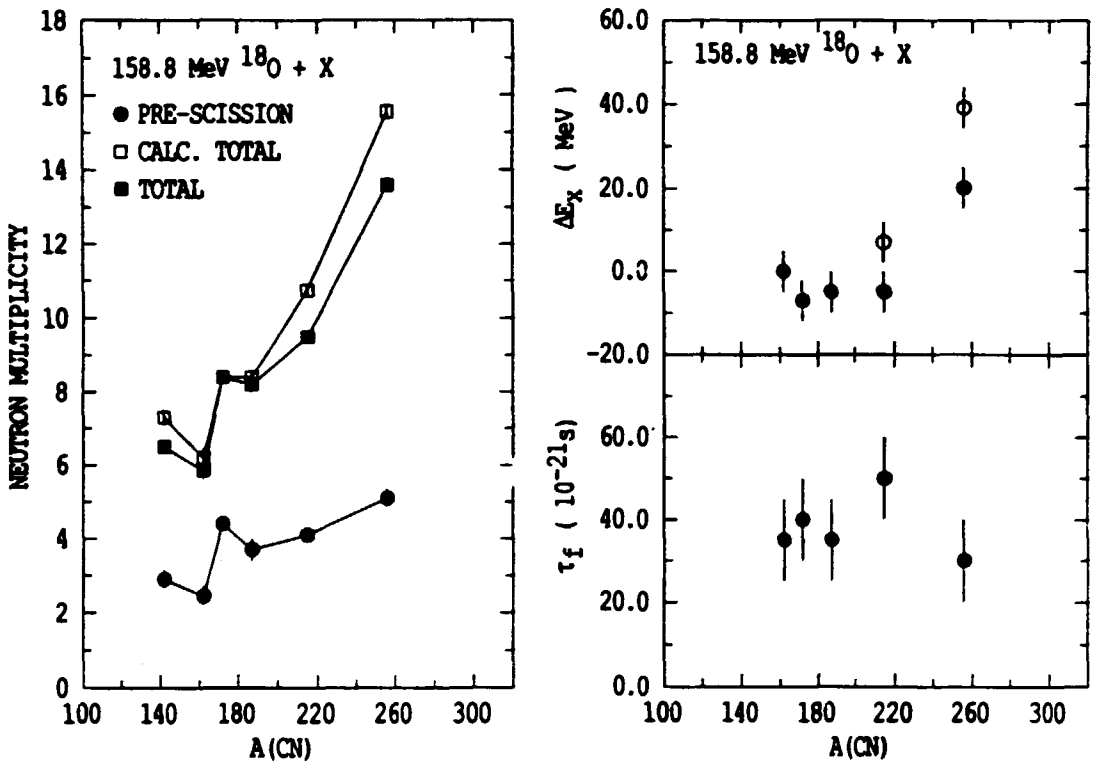


Figure 10: The left panel shows measured $\nu_{pre}$ and $\nu_{tot}$ values, together with calculated $\nu_{tot}$ results. The right panels show the deduced values of $\tau_f$ and $\Delta E_x$ ( see text ).

higher $\Delta E_x$ as shown by the hollow circles; $\tau_f$ is of course unchanged.

The results show $\tau_f$ is centred about 40 $\times$ $10^{-21}$ s, and is independent of fissility within experimental error ( as was concluded with however greater uncertainty by a previous analysis[4] of fusion-fission $\nu_{pre}$ data measured in Japan ). For lighter nuclei, $\Delta E_x$ is $\sim$ -4 MeV, becoming positive for heavier nuclei, a result not inconsistent with expectations based on inspection of Fig.8.

### 4.2 Application To Quasi-Fission

The *neutron clock-thermometer* has been applied to all the experimental data where the experimental errors were sufficiently small to allow a meaningful result. The deduced values of $\Delta E_x$ and $\tau_f$ as a function of mass-split and fragment detection angle for $^{40}$Ar + $^{238}$U are particularly interesting, and are shown in Fig.11. Within error, $\tau_f$ is independent of mass-split, but increases with lab. angle. This is summarised in the right-most panel, where $\tau_f$ increases by more than a factor of two from forward to backward angles. Conversely, $\Delta E_x$ depends on mass, reflecting

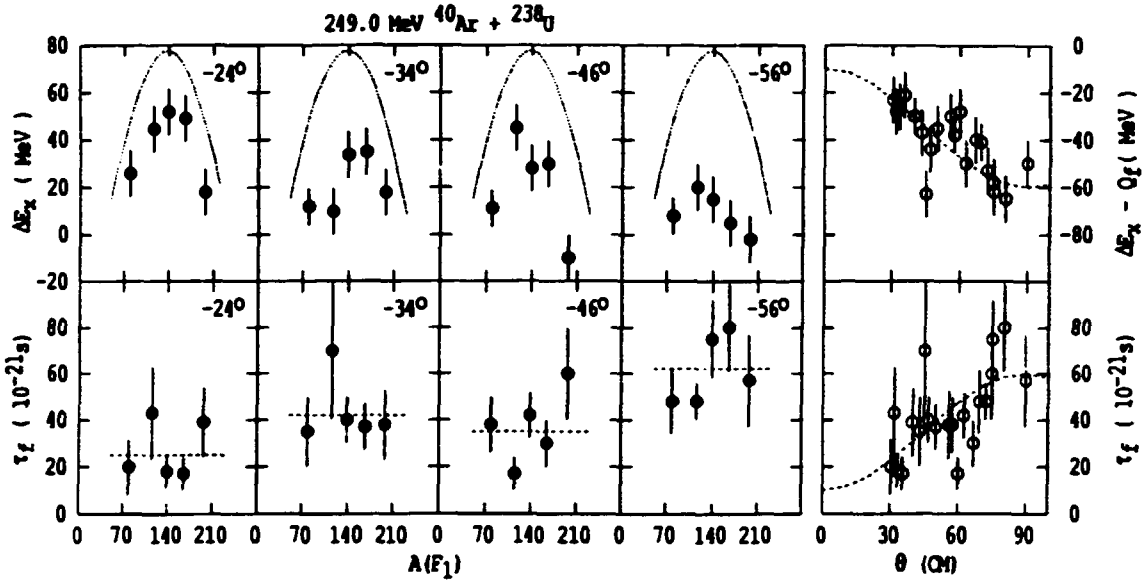


Figure 11: Deduced values of $\tau_f$ and $\Delta E_x$ as a function of the fission fragment mass observed at the indicated lab. angle. The thin dotted lines in the $\Delta E_x$ panels indicate the variation of $Q_f$ with mass, which represents the maximum possible value of $\Delta E_x$ for J = 0. The right-most panels show $\tau_f$ ( below ) and the difference between $\Delta E_x$ and $Q_f$ ( above ) as a function of centre of mass angle, ( see text ). The dashed lines guide the eye.

the variation of $Q_f$ with mass, and also on angle, the latter dependence being summarised in the same way in the right-most panel, decreasing with increasing angle.

This information may be interpreted as follows. Suppose that in the collision process, mononuclei are formed at a range of elongations. The most compact will have the smallest $\Delta E_x$ ( see Fig.8 ), but should live longest, since the distance to scission is greatest. Those formed with more elongated shapes will have the largest $\Delta E_x$ , but the shortest $\tau_f$ , so the fission fragments will be observed at forward angles, but not at 90 degrees, whilst fragments from long-lived mononuclei will be distributed over a much wider range of angles, including 90 degrees.

The above should be treated with some caution due to the likelihood of a correction due to the presence of *acceleration neutrons*; a reduction of all $\nu_{pre}$ values by one would reduce all times by $\sim$ a factor of two ( giving better agreement with times estimated from the deduced rotation angles of the mononuclei ), but it seems unlikely that they could be responsible for all the trends observed in $\tau_f$ and $\Delta E_x$ . Nevertheless, a

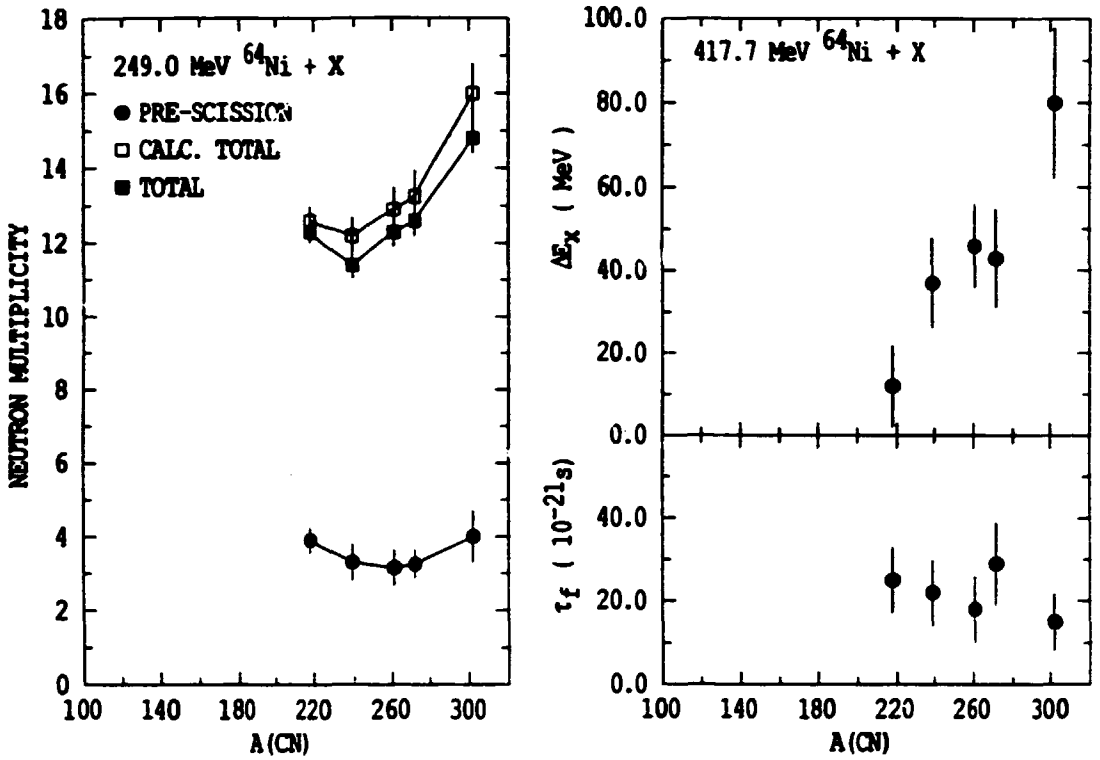


Figure 12: The left panel shows measured $\nu_{pre}$ and $\nu_{tot}$ values, together with calculated $\nu_{tot}$ results. The right panels show the deduced values of $\tau_f$ and $\Delta E_x$ ( see text ).

more quantitative treatment of this effect is clearly desirable.

The application of the *neutron clock-thermometer* to the $^{64}$Ni data may be questionable, since it has already been shown that acceleration neutrons probably contribute very significantly to to apparent $\nu_{pre}$ . Despite this caution, it has been done, applied only to the data for symmetric mass-splits, and the results are shown in Fig.12. The reaction times are $\sim 20\times 10^{-21}$ s, short, but a factor of 3 or 4 longer than estimated by rotation angles for the $^{64}$Ni + $^{238}$U reaction, whilst the values of $\Delta E_x$ approach $Q_f$ . This fact, together with the large contribution expected from emission from the fragments, highlights a problem which is most serious for these $^{64}$Ni data, but which will affect the other analyses to some extent. In our simulation, neutron binding energies, transmission coefficients and level densities used are appropriate for the compound nucleus, but become less and less appropriate the closer the emitter resembles two separated fragments. Indeed, for the $^{64}$Ni reactions, it is almost certainly a better approximation to calculate emission lifetimes for emission from the fragments. Assuming that they are spherical, with no deformation

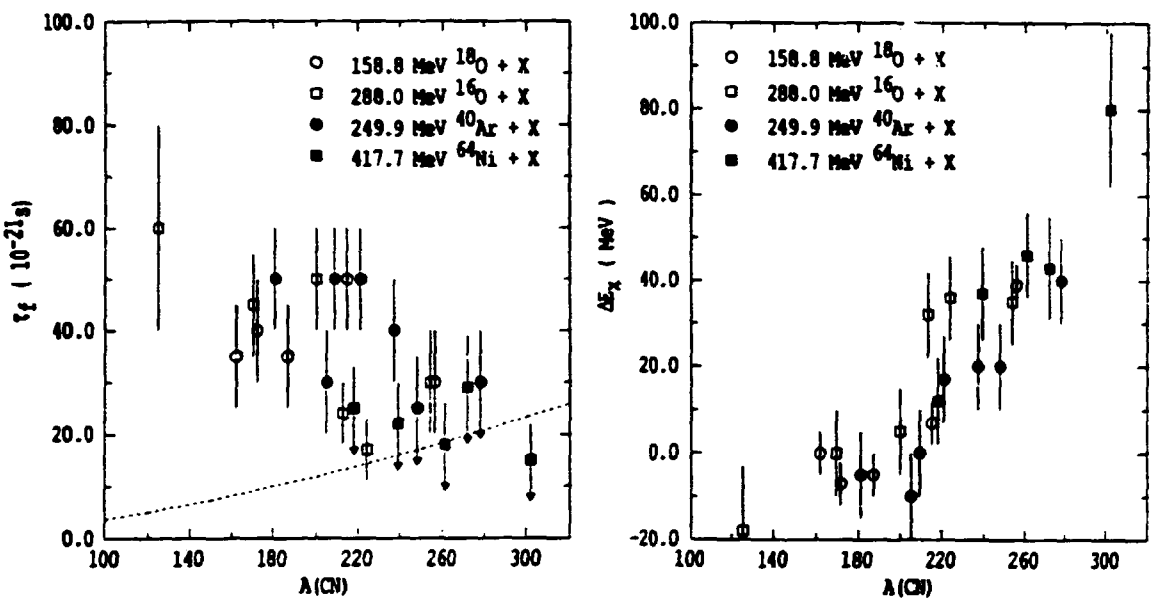


Figure 13: The left panel shows the deduced values of $\tau_f$ for all reactions studied in this work, whilst the right panel shows deduced $\Delta E_x$ . The time for a complete rotation of a nucleus with the moment of inertia of two touching spheres and angular momentum $70\hbar$ is shown by the dashed line in the left panel, all as a function of the compound nucleus mass number A(CN). Downward arrows on the error bars of the $\tau_f$ data indicate quasi-fission reactions where acceleration neutrons are expected to contribute, and inflate the deduced $\tau_f$ value.

energy, gives an upper limit to $E_x$ , and thus a lower limit to calculated times. The measured values of $\nu_{pre}$ for each reaction can be reproduced by allowing emission during a time of $\sim 3 \times 10^{-21}$ s. The true time during which neutron emission will contribute to the measured $\nu_{pre}$ has thus been determined to be between 3 and $20 \times 10^{-21}$ s for these reactions.

## 5 COMPILATION OF RESULTS AND CONCLUSIONS

The results of an analysis of $\nu_{pre}$ and $\varepsilon_{pre}$ values for all fission events in the case of fusion-fission, and for symmetric mass-splits in the cases of quasi-fission are shown in Fig.13. Considering firstly the $\tau_f$ results for fusion-fission ( those for measurements where quasi-fission was observed are signalled by arrow heads on the error bars ), it is very gratifying that for three different experiments, with different kinematic conditions

and detector calibrations, the deduced $\tau_f$ values are so consistent, showing $\tau_f$ is between 20 and 50 $\times$ $10^{-21}$ s. Some questions still remain to be discussed about the influence of acceleration neutrons for the most neutron-rich heavy nuclei, and the influence of fast-fission ( fission without barrier ); it may be that data with higher statistical accuracy are required to permit definitive conclusions to be drawn from experimental data alone. It must be recalled that the $\tau_f$ deduced in this analysis for the fusion-fission data are for a complete suppression of fission during $\tau_f$ . Thus $\tau_f$ is not equivalent to the pre-saddle delay time in a model in which the fission width rises gradually to it's asymptotic value, since in the case of a low fission barrier and thus high fission width, fission may compete equally with neutron emission well before the full fission width is reached.

The $\Delta E_x$ data again show a remarkable clustering, indeed the agreement for heavy nuclei of fusion-fission and quasi-fission data points is surprising, and points to the need for analysis of the $\nu_{pre}$ and $\epsilon_{pre}$ data by a more sophisticated dynamical/evaporation simulation of fission. The slope of $\Delta E_x$ with A(CN) follows the variation of $Q_f$ quite closely, however this may be partly due to the choice of $a_n$ . It would clearly be useful if the prescription used for $a_n$ were tested experimentally, so that the interpretation of $\Delta E_x$ could proceed with less uncertainty. Independent of this, it is however clear that $\epsilon_{pre}$ , and the neutron energy spectra in general carry very useful information, which should not be neglected.

Turning to the raw neutron multiplicity data, the marked dependence of $\nu_{pre}$ on mass-asymmetry in fusion-fission, and the dependence on TKE in quasi-fission have been clearly shown for the first time.

The interpretation of the former in terms of a dependence of the fission time scale on mass-asymmetry is of importance in the development of a unified picture of binary decay, including both fission and evaporation.

The latter may be useful, in conjunction with better simulations of evaporation from the nucleus near and after scission, in allowing a calibration of the *neutron clock* against the reaction time and acceleration time of the fragments. The very fact that $\nu_{pre}$ shows such a strong dependence on TKE indicates that the scission configuration is compact, with little deformation energy, since the difference in available energy due to the different TKE values seems to be largely felt in the thermal energy,

available for neutron emission.

The lack of dependence of $\nu_{pre}$ on TKE for fusion-fission can be taken as evidence for the unimportance of emission after the TKE has been decided in these reactions.

The use of both $\nu_{pre}$ and $\epsilon_{pre}$ data in the interpretation of neutron measurements in fission clearly represents a significant advance, and in conjunction with the new results obtained as a function of mass-split and TKE, should act as a spur to further measurements in this field, not only of neutrons, but also of charged particles, $\gamma$-rays and fission probabilities[14,15].

Statistical model calculations with the code JULIAN were performed on the Fujitsu VP100 of the Australian National University Supercomputer Facility.

## REFERENCES

1) D. J. Hinde et al., Nucl. Phys. A502(1989)497c, and references therein
2) G. F. Peaslee et al., Phys. Rev. C38(1988)1730, and references therein,
H. Ikezoe et al., Phys. Rev. C42(1990)342,
J. P. Lestone et al., submitted to Phys. Rev. Lett.
3) M. Thoennessen et al., Phys. Rev. Lett. 59(1987)2860
4) D. J. Hinde et al., Phys. Rev. C39(1989)2268
5) H. Rossner et al., Phys. Rev. C43(1991)2434
6) V. E. Viola et al., Phys. Rev. C31(1985)1550
7) R. J. Charity et al., Nucl. Phys. A483(1988)371
8) U. Lynen et al., Phys. Rev. Lett. 59(1987)2844
9) J. Pochodzalla et al., Phys. Rev. C40(1989)2918
10) L. G. Moretto and G. Wozniak, Pramāṇa - J. Phys. 33(1989)209
11) J. Tōke et al., Nucl. Phys. A440(1985)327
12) D. J. Hinde et al., Phys. Rev. Lett. 52(1984)986, 53(1984)2275(E)
13) J. Tōke and W. Swiatecki, Nucl. Phys. A372(1981)141
14) M. Gonin et al., Nucl. Phys. A495(1989)139c
15) E.-M. Eckert et al., Phys. Rev. Lett. 64(1990)2483